Bioinspired Silicification of Functional Materials: Fluorescent Monodisperse Mesostructure Silica Nanospheres

ARTICLE *in* CHEMISTRY OF MATERIALS · DECEMBER 2009

Impact Factor: 8.35 · DOI: 10.1021/cm9031013

4 AUTHORS, INCLUDING:

Rohit Kumar Rana
Indian Institute of Chemical Technology
52 PUBLICATIONS **1,062** CITATIONS
SEE PROFILE

Shashi Singh
Centre for Cellular and Molecular Biology
74 PUBLICATIONS **2,564** CITATIONS
SEE PROFILE

CHEMISTRY OF MATERIALS
Article

Chem. Mater. **2010,** *22,* 551–556 551
DOI:10.1021/cm9031013

Bioinspired Silicification of Functional Materials: Fluorescent Monodisperse Mesostructure Silica Nanospheres

Gousia Begum,[†] Rohit K. Rana,*[,†] Shashi Singh,[‡] and L. Satyanarayana[†]

[†]*Nanomaterials Laboratory, Inorganic and Physical Chemistry Division, Indian Institute of Chemical Technology, Hyderabad-500 607, India and* [‡]*Centre for Cellular and Molecular Biology, Hyderabad- 500 007, India*

Received October 7, 2009. Revised Manuscript Received December 10, 2009

Herein we demonstrate a simple but versatile bioinspired polyamine-catalyzed silicification route to synthesizing functional materials which is monodisperse, mesoporous, and spherically uniform having nanosizes under extremely mild conditions similar to the biosilicification processes. Employing the principles learned from nature and in particular from diatom biomineralization to integrate the functions required for silica condensation and self-assembly leads to the formation of such functional materials. Importantly, the integration of such functions requires the presence of suitable multivalent counteranions, whose interaction is structure specific while facilitating the mineralization process to form these unique silica structures under the green conditions of aqueous medium, neutral pH, and room temperature. The versatility of the method is exemplified in controlling the size, uniformity, and the nanoarchitectural features of the silica obtained within a very short time frame of 30 min. A wide variety of techniques (fluorescence imaging, live confocal imaging, dynamic light scattering, MAS ^{29}Si NMR, N_2 sorption, X-ray diffraction, FT-IR, thermo-gravimetric analysis, scanning and transmission electron microscopy) have been used to study the formation process and characterization of the materials.

Introduction

Inspired by the ability of diatoms to grow beautiful and complicated skeletons of silica under green conditions, much recent work has been devoted on the chemical approach to produce similar results.[1,2] The real breakthrough came from Sumper et al. who showed that the silaffins, a set of cationic polypeptides isolated from the diatom *cylindrotheca fusiformis*, can precipitate silica spheres from aqueous silicic acid in vitro.[3] Similarly silicatein−a protein found in the silica spicules of the sponge *Tethya aurantia* can hydrolyze and condense TEOS (tetraethylorthoslicate) to form silica structure at ambient conditions.[4,5] Further investigations have shown that polyamines and specifically designed amine-containing compounds have ability for silica condensation, but due to their limited self-assembly properties achieving structural features in the nanometer range has been difficult.[6−8] The obtained structures mainly include polydispersed spheres, hexagonal platelets, and a few other morphologies without much morphological homogeneity.[9−18] This has been our motivation to explore the biosilicification knowledge further to develop new methodologies for synthesizing materials with controllable uniform sizes and nanoarchitectural features.[19,20] Here, for the first time, we demonstrate a bioinspired polyamine-catalyzed silicification route to synthesize monodisperse mesoporous silica nanospheres (MMSN) under extremely mild conditions. Use of fluorescent-tagged polyamines as silicification mineralizer straightaway affords the formation of fluorescent monodisperse mesoporous silica nanospheres in a single step.

*Author to whom correspondence should be addressed. E-mail: rkrana@iict.res.in.

(1) Bauerlein, E. *Angew. Chem., Int. Ed.* **2003**, *42*, 614–641.
(2) Halas, N. J. *ACS Nano* **2008**, *2*, 179–183.
(3) Kroger, N.; Deutzmann, R.; Sumper, M. *Science* **1999**, *286*, 1129–1132.
(4) Brutchey, R. L.; Morse, D. E. *Chem. Rev.* **2008**, *108*, 4915–4934.
(5) Coradin, T.; Livage, J. *Acc. Chem. Res.* **2007**, *40*, 819–826.
(6) Kessel, S.; Thomas, A.; Börner, H. G. *Angew. Chem., Int. Ed.* **2007**, *46*, 9023–9026.
(7) Menzel, H.; Horstmann, S.; Behrens, P.; Bärnreuther, P.; Krueger, I.; Jahns, M. *Chem. Commun.* **2003**, 2994–2995.
(8) Knecht, M. R.; Wright, D. W. *Langmuir* **2004**, *20*, 4728–4732.
(9) Bellomo, E. G.; Deming, T. J. *J. Am. Chem. Soc.* **2006**, *128*, 2276–2279.
(10) Ford, J.; Yang, S. *Chem. Mater.* **2007**, *19*, 5570–5575.
(11) Sun, Q.; Vrieling, E. G.; Van Santen, R. A.; Sommerdijk, N. A. J. M. *Curr. Opin. Solid State Mater. Sci.* **2004**, *8*, 111–120.
(12) Chang, J-S.; Kong, Z-L.; Hwang, D-F.; Chang, K. L. B. *Chem. Mater.* **2006**, *18*, 702–707.
(13) Hawkins, K. M.; Wang, S. S. S.; Ford, D. M.; Shantz, D. F. *J. Am. Chem. Soc.* **2004**, *126*, 9112–9119.
(14) Patwardhan, S. V.; Clarson, S. J.; Perry, C. C. *Chem. Commun.* **2005**, *9*, 1113–1121.
(15) Dickerson, M .B.; Sandhage, K. H.; Naik, R. R. *Chem. Rev.* **2008**, *108*, 4935–4978.
(16) Zhou, F.; Li, S.; Vo, C. D.; Yuan, J.-J.; Chai, S.; Gao, Q.; Armes, S. P.; Lu, C.; Cheng, S. *Langmuir* **2007**, *23*, 9737–9744.
(17) Jin, R.-H.; Yuan, J.-J. *Chem. Commun.* **2005**, 1399–1401.
(18) Corma, A.; Díaz-Cabañas, M. J.; Moliner, M.; Rodríguez, G. *Chem. Commun.* **2006**, 3137–3139.
(19) Begum, G.; Manorama, S. V.; Singh, S.; Rana, R. K. *Chem .Eur. J.* **2008**, *14*, 6421–6427.
(20) Rana, R. K.; Murthy, V. S.; Yu, J.; Wong, M. S. *Adv. Mater.* **2005**, *17*, 1145–1150.

Published on Web 12/30/2009

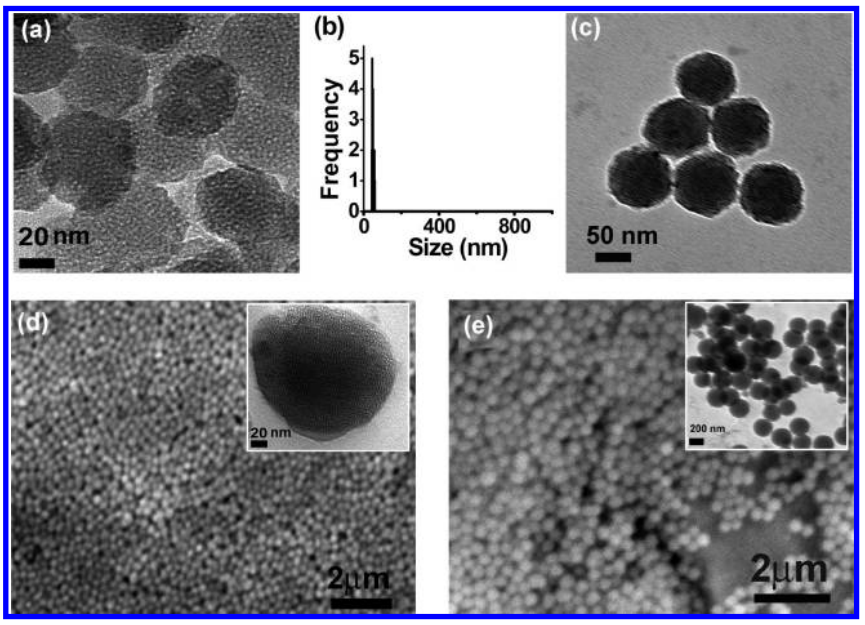

Figure 1. TEM image and corresponding particle size distribution plots from DLS analysis for the (a, b) Sample 1; (c) TEM image of Sample 4; (d) SEM images of the Sample 2 (inset HRTEM of microtomed slice), and (e) SEM images of the Sample 3 (inset TEM image). Sample 2 was aged for 15 h and Samples 1, 3, and 4 were aged for 30 min.

On the contrary, the laboratory method of surfactant mediated synthesis of mesoporous silica in monodisperse spherical form require either exclusively modified surfactants or extreme pH or high temperature, and the time required for the preparation is usually several hours to days.[21−35] Also, often particle coalescence is a major problem resulting in polydispersity and irregular shapes. So, it is highly important to have environmentally benign production of mesoporous silica with high surface area and well-dispersed uniform colloids in nanometer sizes. In this regard, the bioinspired silicification method can be simply an attractive alternative to other synthetically produced mesoporous silica.

Results and Discussion

Synthesis and Characterization. The biomolecules found in biosilica are believed to perform two indispensable functions. They are capable of catalyzing silica condensation, as well as forming macromolecular assemblies that are assumed to act as structure-directing templates. To integrate both the functionalities into our approach, we combined polyamines as mineralizer with cationic surfactant *N*-cetyl-*N*,*N*,*N*-trimethyl ammonium bromide (CTAB) to serve as supramolecular templates in presence of multivalent anions. Polyallylamine (PAH), which is a long-chain polyamine similar to that found in diatoms, was chosen for silica formation. The positively charged PAH can cross-link with citrate ions to form spherical aggregates.[36,37] These aggregates further catalyze silicic acid (freshly prepared from tetramethyl orthosilicate, Supporting Information (SI)) condensation generating polydisperse silica spheres of 0.8−3.0 μm sizes (SI Figure S1). However, when the same reaction was carried out in presence of CTAB, quite contrastingly, monodisperse spherical silica particles in the nanometer range (MMSN) were obtained.

The TEM image in Figure 1a shows monodisperse spheres of ∼50 nm size obtained with a CTAB concentration of 0.04 M. The mesoporous structure of individual nanospheres is also clearly visible in the image. For a lower CTAB concentration the size of the MMSN increased as evident from the TEM and SEM images (Figure 1d). The uniformity and monodispersity of the particles could be improved further with increase in concentration of the silica precursor (Figures 1c and e). HRTEM of microtomed sample reveals the mesoporous architecture spreading throughout the sphere (Figure 1d inset).

(21) Han, Y; Ying, J. Y. *Angew. Chem., Int. Ed.* **2005**, *44*, 288–292.
(22) Büchel, G.; Grün, M.; Unger, K. K.; Matsumoto, A.; Tsutsumi, K. *Supramol. Sci.* **1998**, *5*, 253.
(23) Yamada, Y.; Yano, K. *Microporous Mesoporous Mater.* **2006**, *93*, 190–198.
(24) Boissiere, C.; Lee, A. V.; El Mansouri, A.; Larbot, A.; Prouzet, E. *Chem. Commun.* **1999**, 2047–2048.
(25) Fowler, C. E.; Khushalani, D.; Lebeau, B.; Mann, S. *Adv. Mater.* **2001**, *13*, 649–652.
(26) Suzuki, K.; Ikari, K.; Imai, H. *J. Am. Chem. Soc.* **2004**, *126*, 462–463.
(27) Rao, G. V. R.; Lopez, G. P.; Bravo, J.; Pham, H.; Datye, A. K.; Xu, H.; Ward, T. L. *Adv. Mater.* **2002**, *14*, 1301–1304.
(28) Carroll, N. J.; Rathod, S. B.; Derbins, E.; Mendez, S.; Weitz, D. A.; Petsev, D. N. *Langmuir* **2008**, *24*, 658–661.
(29) Pang, J.; Na, H.; Lu, Y. *Microporous Mesoporous Mater.* **2005**, *86*, 89–95.
(30) Nooney, R. I.; Thirunavukkarasu, D.; Chen, Y.; Josephs, R.; Ostafin, A. E. *Chem. Mater.* **2002**, *14*, 4721–4728.
(31) Rana, R. K.; Mastai, Y.; Gedanken, A. *Adv. Mater.* **2002**, *14*, 1414–1418.
(32) Kobler, J .; Möller, K.; Bein, T. *ACS Nano* **2008**, *2*, 791–799.
(33) Derrien, G.; Charnay; Zajac, J.; Jones, D. J.; Rozière, J. *Chem. Commun.* **2008**, 3118–3120.
(34) Puchol, V.; Haskouri, J. E.; Latorre, J.; Guillem, C.; Beltra′n, A.; Beltra′n, D.; Amoro′s, P. *Chem. Commun.* **2009**, 2694–2696.
(35) Berggren, A.; Palmqvist, A. E. C. *J. Phys. Chem. C* **2008**, *112*, 732–737.
(36) Murthy, V. S.; Rana, R. K.; Wong, M. S. *J. Phys. Chem. B* **2006**, *110*, 25619–25627.
(37) Brunner, E.; Lutz, K.; Sumper, M. *Phys. Chem. Chem. Phys.* **2004**, *6*, 854–857.

Table 1. Morphological Properties of the Silica Particles Obtained under Various Reaction Conditions.

sample	molar ratio citrate: PAH: CTAB: silicic acid	shape[a]	dispersity[a]	particle diameter (nm)[b]
1	0.14: 0.05:1.2: 1	spherical	monodisperse	45 ± 5 (50 ± 3)
2	0.14: 0.05: 0.6: 1	spherical	monodisperse	230 ± 8 (240 ± 8)
3	0.14: 0.05: 0.6: 5	spherical	monodisperse	250 ± 8
4	0.14: 0.05:1.2: 5	spherical	monodisperse	80 ± 5
5	0.14: 0.05: 0.3: 1	agglomerated spheres	polydisperse	>250
6	0.14: 0: 0.6: 1	spheres and plates	polydisperse	>400
7 [c]	0.14: 0.05: 0: 1	spherical	polydisperse	800−3000

[a]The shape and dispersity remain the same for the sample aged for 30 min and 15 h. [b]Particle diameters are calculated from TEM images and the data within parentheses are for 15 h aging time, whereas all others are for 30 min aging time. [c]Sample 7 after aging for 15 h resulted in gel.

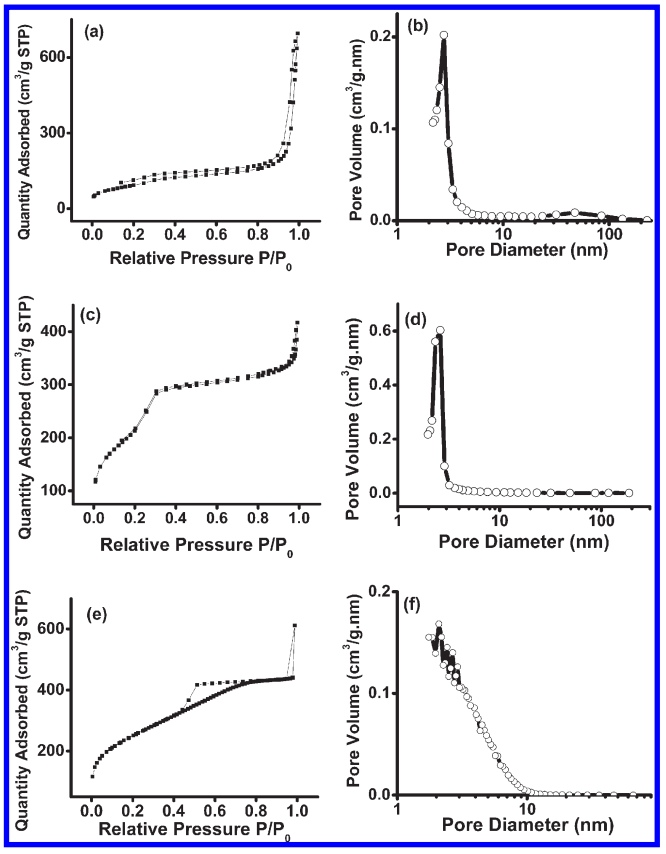

Figure 2. N_2 sorption isotherms and the corresponding BJH pore size distribution plots, respectively for Sample 1 aged for (a, b) 15 h ; (c, d) Sample 2 aged for 15 hrs, and (e, f) Sample 7 aged for 30 min.

The pores are of open-type having accessibility from the surface with an average pore diameter of ~2.4 nm. The particle morphology and mesoporous structure remained intact even after the removal of the organic contents by calcination (SI Figure S2). But, as the CTAB concentration was further lowered, highly agglomerated spheres were formed (SI Figure S3) indicating that there is an optimum CTAB concentration in which well-dispersed MMSN are formed.

The mode of addition of each reagent and the concentrations of PAH and citrate buffer were also found to influence the final structure (SI Figures S4−S6). Here it is worth mentioning that none of the PAH and CTAB individually or together in absence of citrate are capable of condensing silicic acid at pH 7. Even the citrate buffer does not precipitate silica. It is only in presence of citrate buffer either individually or together with PAH and CTAB condense silica. In case of PAH the role of citrate is to ionically assemble the PAH chains so that the ammonium groups bring silicate ions sufficiently close to each other for condensation to occur forming a silicate network.[38] Similar results were obtained when poly(L-lysine) was used in place of PAH keeping all other parameters constant (SI Figure S7). On the other hand, the citrate ions can also assist CTAB undergoing cooperative self-assembly with silicic acid to form mesostructure silica as known for certain counter-ions that can influence the morphological transition of CTAB from spherical to cylindrical micelles.[39,40] However, in both the above cases, the silica particles formed were polydisperse in their sizes (SI Figure S1 and Table 1) indicating that a cumulative effect of all the components is required to form MMSN.

The XRD patterns of MMSN samples (SI Figure S8) show two well resolved low-angle peaks indexed to 100 and 110 reflections corresponding to the 2D−hexagonal *p6mm* space group of MCM-41[41] which confirms the existence of a mesostructure with approximately uniform pore sizes. The absence of any higher order reflections indicates limited periodicity in the long-range ordering of the pores. The N_2-sorption on the calcined MMSN reveal an isotherm (Figure 2 and SI Figure S9), which can be assigned to type IV typical of mesoporous materials with a high specific surface area of 700−1000 m^2g^{-1} (SI Table S1) and pore volume of 0.6−0.9 cm^3g^{-1}. The BJH (Barret−Joyner−Halenda) analysis of MMSN shows the existence of mesopores averaging at 2.2−2.7 nm with a narrow distribution (Figure 2(b and d) and SI Figure S9). Interestingly, Sample 1 exhibits another pore centered at 48 nm having a broad distribution attributed to the textural porosity present between nanometer sized spheres.[42,43] In the case of Sample 7, the absence of CTAB resulted in a broad pore size distribution (< 4.0 nm) mainly due to the conformation assumed by the polyamines inside the silica matrix.[13] This clearly indicates that the CTAB is primarily responsible for the narrow size distribution of the mesopores in MMSN.

(38) Coradin, T.; Durupthy, O.; Livage, J. *Langmuir* **2002**, *18*, 2331–2336.
(39) Xiao, Q.; Wang, J.; Zhou, H.; Sun, P.; Yuan, Z.; Li, B.; Ding, D.; Chen, T. *Microporous Mesoporous Mater.* **2008**, *109*, 233–238.
(40) Lin, H. P.; Kao, C. P.; Mou, C. Y.; Liu, S. B. *J. Phys. Chem. B* **2000**, *104*, 7885–7894.
(41) Che, S.; Lim, S.; Kaneda, M.; Yoshitake, H.; Terasaki, O.; Tatsumi, T. *J. Am. Chem. Soc.* **2002**, *124*, 13962–13963.
(42) Cai, Q.; Luo, Z -S.; Pang, W -Q.; Fan, Y -W.; Chen, X -H.; Cui, F -Z. *Chem. Mater.* **2001**, *13*, 258–263.
(43) Tanev, P. T.; Pinnavaia, T. J. *Chem. Mater.* **1996**, *8*, 2068–2079.

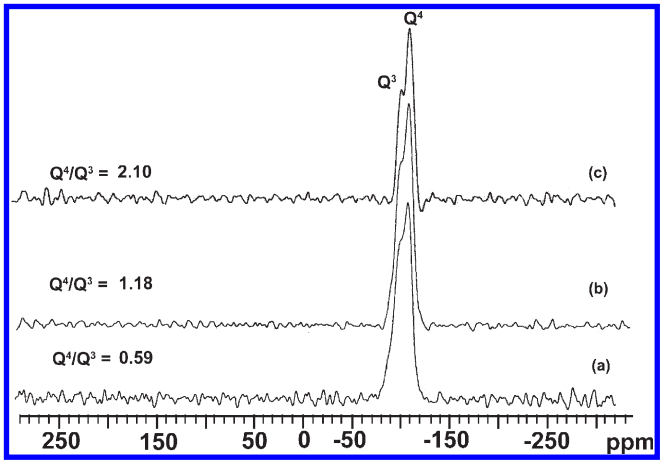

Figure 3. MAS ^{29}Si NMR spectra and their corresponding Q^4/Q^3 ratios for the as-synthesized (a) Sample 7, (b) Sample 1, and (c) Sample 3. All the samples were obtained with aging time of 30 min.

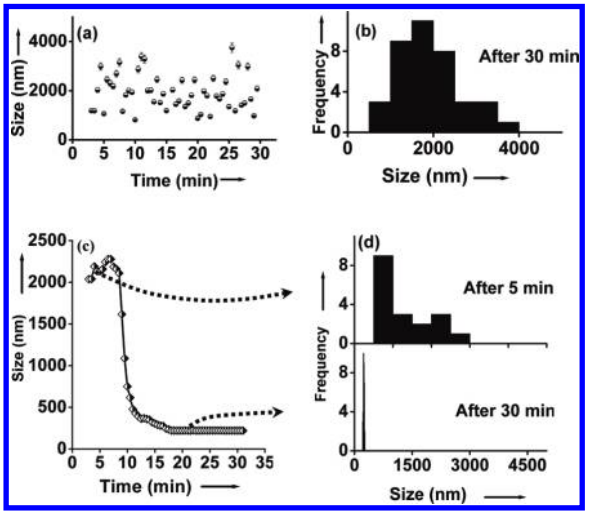

Figure 4. DLS measurements of variation in hydrodynamic diameter with aging time and the corresponding size distribution for (a and b) Sample 7 and (c and d) Sample 2, respectively.

The presence of the organic components in MMSN samples was confirmed from FT-IR analysis (SI Figure S10). TGA analysis showed that the silica yield for the MMSN samples increases with the aging time though the increase is not very high (SI Table S2 and Figure S11). Since within 30 min of the reaction ~51% of silicic acid (~0.031 M) is already utilized, the remaining concentration of silicic acid becomes low (~0.015 M) and in addition as discussed below, the PAH which helps in mineralizing silica is also completely consumed in the silica formation. Both eventually slow down the silica condensation. Even after 60 h of aging the yield was ~86% (SI Figure S12). As seen in SI Table S2, the presence of CTAB in the system also improves the silica yield. Thus the CTAB has a role in silica condensation apart from imparting the mesostructure. This was further supported by the MAS ^{29}Si NMR spectra of the as-synthesized samples which exhibited mainly two peaks at −101 (Q^3) and −110 (Q^4) ppm corresponding to silicon with three and four siloxane bonds, respectively (Figure 3 and SI Figure S13), indicating a relatively high degree of cross-linking of silica. A higher Q^4/Q^3 ratio was observed for all the samples having CTAB as a component than that obtained with only PAH. Nevertheless, it is the cooperative interaction of CTAB and PAH which results in efficient condensation of silicic acid, hence higher Q^4 for MMSN, which increases with increase in the amount of silica precursor (Sample 3).

DLS measurements showed that as the silicic acid was added to a suspension of PAH−citrate aggregates it resulted in silica spheres having the sizes varying between 0.8 and 3.5 μm with time (Figure 4a and b). The sizes and the dispersity of the silica spheres were similar to that of initially formed PAH−citrate aggregates. In Sample 2, when CTAB was added to the PAH−citrate aggregates, it neither changed the size nor the polydispersity. But with addition of silicic acid to the above PAH−citrate−CTAB mixture, a sharp change in sizes with time was observed (Figure 4c and d). In the initial stage (< 10 min) the average size remained within 2.0−2.5 μm and the size distribution was less broad. Then after 10 min a sharp decrease in the size down to nanometer range was observed after which it reached a plateau. This fact is further supported by the fluorescence microscopic analyses to track the location of PAH by tagging it with FITC. Figure 5 shows that as the time passed smaller spheres appeared while both the size and the number of micrometer-sized spheres gradually decreased. This is quite noticeable in the live confocal imaging experiment (Figure 6). The overlay image in Figure 5f (inset) clearly shows that the PAH molecules are entrapped inside the MMSN. It is known that most of the polyamine is utilized in making the micron-sized silica spheres in case of Sample 7.[20] From UV−vis spectroscopic analysis we estimated that ~95% of FITC tagged PAH is consumed in the formation PAH−citrate aggregates, whereas further addition of CTAB and silicic acid resulted in complete utilization of FITC-PAH forming silica nanospheres (MMSN) (SI Figure S14). Therefore, in case of Sample 2 it is plausible that during the course of reaction the FITC tagged PAH disassembles from the bigger polymer aggregates and then reassembles with CTAB and silicic acid to form smaller and uniform silica spheres so as to make them fluorescent. Since the assembly of PAH with citrate is responsive to change in pH or ionic strength,[36] the above disassembly process might be influenced by the addition of CTAB and silicic acid solutions. A similar trend was also observed for other samples and with PAH of different M.Wt. (SI Figures S15 and S16).

Furthermore, to understand the above process, the role of anionic cross-linker was investigated. When citrate was replaced with phosphate ions, contrastingly micron size polydisperse silica spheres were obtained and the particles did not exhibit any mesostructure ordering (SI Figure S17). This implies that unlike citrate the PO_4^{3-} ions are not capable of inducing CTAB to condense silica from silicic acid, and hence the silica condensation was mainly catalyzed by PAH−PO_4^{3-} aggregates resulting in micron sized silica spheres. This was verified from the observation that CTAB and PO_4^{3-} mixture does not condense silicic acid at

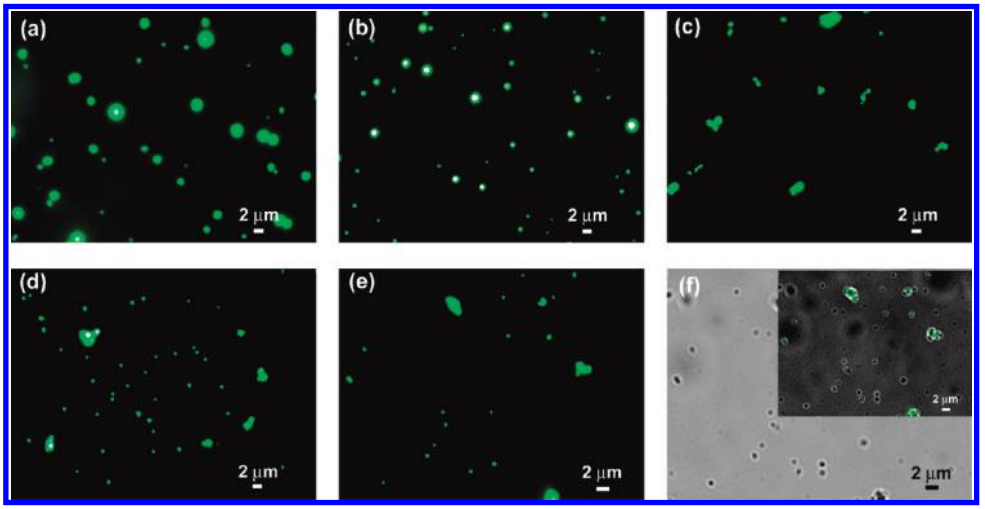

Figure 5. Fluorescence images of the samples obtained with FITC tagged PAH; (a) PAH−citrate aggregate after 30 min aging; (b−e) PAH−Cit−CTAB-silicic acid mixture (Sample 2) after aging for (b) 5 min, (c) 15 min, (d) 30 min, and (e) 40 min; Few big particles in (d and e) are actually agglomerates of smaller spheres as seen in the bright field image (f) of the 40 min aged sample. The inset in (f) represents the overlay image of (e) and (f).

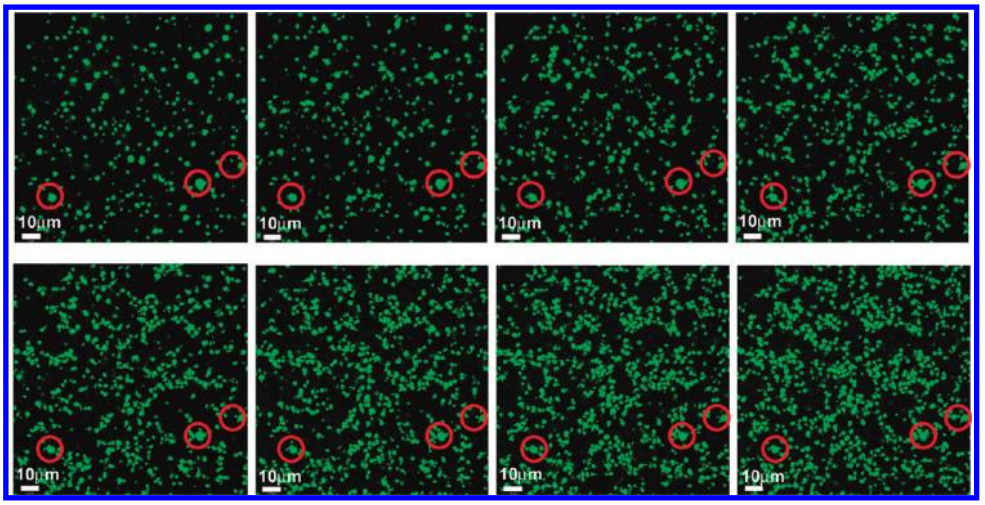

Figure 6. Live confocal imaging to follow the synthesis of Sample 3. The first picture is of PAH−citrate aggregates after 30 min aging. After the addition of CTAB and silicic acid to the above mixture, pictures were taken at 6 min intervals. As the experiment was performed with a glass coverslip placed at the bottom of a sample chamber, some of the initially formed PAH−citrate aggregates got stuck to the coverslip (indicated by circles). So after the addition of CTAB and silicic acid to the same chamber, these bigger aggregates did not undergo much change in their sizes with time. But it was clearly seen that as the reaction proceeded there was no further appearance of any bigger spheres other than the stuck ones and with time more and more silica particles of smaller size were formed.

Scheme 1. Schematic Illustration of the Nucleation and Growth Processes Involved in the Formation of Mesoporous Monodisperse Silica Nanospheres

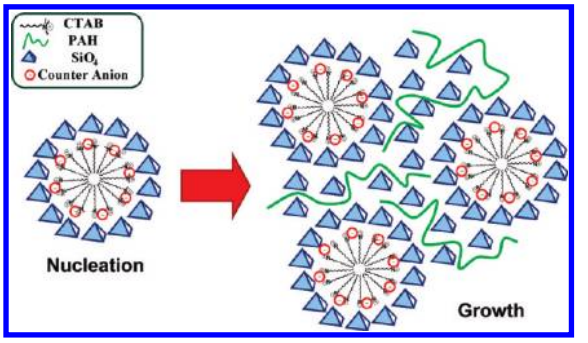

the neutral pH. In addition, use of monovalent anions such as NO_3^- and acetate was not successful in enabling CTAB to precipitate silica even after two days of aging. So, the function of multivalent anions is very crucial and structure-specific in interacting with CTAB, which in turn generates the nucleating sites for the formation of MMSN particles (Scheme 1). A similar structure-specific interaction of polyamine with anions is known as well.[36,37]

The fact that PAH is entrapped in MMSN suggests that the cationic PAH chains are incorporated into the negatively charged silicate framework during the condensation process driven by an electrostatic interaction (Scheme 1). As a consequence the PAH−citrate aggregates start disassembling and then rearrange themselves in the mesophase of CTAB-silica structure. The entrapped PAH seems to have a major role in the silica growth process as the formed spheres are both monodisperse and smaller in size only when the PAH is present. This is possible if the presence of PAH can slow down the growth rate so that the particles reach an equilibrium monodisperse size. Otherwise, if the growth rate is high it should lead to irregular growth of silica from the nuclei

and thereby forming particles with varied sizes and shapes.[44] This was the case in absence of PAH where the CTAB−citrate system generates both spheres and plate like structures (SI Figure S1(b)). A recent study has shown that increased alkylation of an amine significantly enhances their silica condensing capacity.[45] This is in agreement with the above explanation that the assembled CTAB having quaternary ammonium groups would have a greater reactivity than PAH to condense silica. This indeed is reflected in the silica yields as less amount of silica formed with PAH than without PAH (SI Table S2). Therefore, the role of PAH is not only to help in condensing silica from silicic acid but also to control the rate of silica growth. The PAH molecules may also cover the surface of the silica spheres to prevent inter particle coalescence forming a stable colloidal sol.

Conclusions

In summary, we have demonstrated that the polyamine-catalyzed silicification process can be suitably modified to synthesize functional materials. An unique integration of the two central biosilicification principles, that is, the polyamine-catalyzed silica condensation and the supramolecular structure directing effect leads to mineralization of monodisperse mesoporous silica nanospheres under the green conditions similar to the biosilicification processes. The result brings out a new phenomenon that the multivalent counteranions play a critical role in self-organizing both the polyamines and cationic surfactants. Interestingly, this interaction is structure specific while facilitating the mineralization process to form such unique silica structures under the mild conditions of aqueous medium, neutral pH, and room temperature. Further, the biomimetic approach suggests that the principles learned from diatom biomineralization can be judiciously utilized to get useful functional materials and hence provides great potential for developing green processes to obtain structured materials of nanometer dimensions for various applications.

Experimental Section

Synthesis of Monodisperse Mesoporous Silica Nanospheres (MMSN). For the synthesis of monodisperse mesoporous silica spheres, the various molar compositions tried are tabulated in Table 1. Typically to 100 μL of 5−40 mM citrate buffer 16.6 μL of 2−10 mg/mL PAH (15 KDa, and 70 KDa) was added which led to a turbid suspension. After it was aged for half an hour, a mixture containing 43.4 μL of 0.05−0.2 M CTAB and 72.4 μL of 0.1−0.5 M silicic acid was added. It was then aged for 30 min to 60 h with constant stirring at room temperature. CTAB and silicic acid were mixed immediately before their addition to the PAH−citrate aggregates. Here it should be noted that the results were same when CTAB was added followed by silicic acid in a stepwise manner. The pH of the solution through out the synthesis remained in between 6.5 and 7.0. Initially the reaction was carried out in μL scale but for further characterizations by DLS, XRD and N_2-sorption the reaction was carried out in mL scale (total volume of 240 mL) with the same molar ratio as above. The resulted silica precipitates were centrifuged and washed several (5−6) times with deionized water and dried at room temperature. To remove the organic content the samples were calcined at 550 °C for 4 h at a heating rate of 2 °C min^{-1}. To obtain fluorescent monodisperse mesoporous silica nanospheres (FMMSN) FITC-tagged PAH was used as the mineralizer instead of only PAH. Similarly, poly(L-lysine) was also tested for the formation of MMSN keeping all other parameters same. In a separate experiment the citrate buffer was replaced by phosphate buffer, acetate buffer, and nitrate ions to study the effect of counterions.

Acknowledgment. Financial support from DST, India (Fast-Track) and CSIR, India (Network project on "Nanomaterials and Nanodevices") and UGC, India are greatly acknowledged. we are grateful to Dr. S.V. Manorama, Nandini Rangaraj, Dr. R. Baneerjee, S. L. Ralte, J. Bhattacharyya, C. Subbalakshmi, and Dr. V. R. Rao for their help in material characterization.

Supporting Information Available: Detail experimental, analyses by TEM, SEM, XRD, FT-IR, TG-DTA, N_2 sorption, DLS, NMR and UV−vis spectroscopy. This material is available free of charge via the Internet at http://pubs.acs.org.

(44) Hartlen, K. D.; Athanasopoulos, A. P. T.; Kitaev, V. *Langmuir* **2008**, *24*, 1714–1720.
(45) Robinson, D. B.; Rognlien, J. L.; Bauer, C. A.; Simmons, B. A. *J. Mater. Chem.* **2007**, *17*, 2113–2119.